The EMBO Journal Vol.16 No.6 pp.1181–1188, 1997

Projection structure of the cytochrome *bo* ubiquinol oxidase from *Escherichia coli* at 6 Å resolution

Ulrich Gohlke, Antony Warne and Matti Saraste

European Molecular Biology Laboratory, Biological Structures Programme, Meyerhofstrasse 1, Postfach 10.2209, D-69012 Heidelberg, Germany

The haem–copper cytochrome oxidases are terminal catalysts of the respiratory chains in aerobic organisms. These integral membrane protein complexes catalyse the reduction of molecular oxygen to water and utilize the free energy of this reaction to generate a transmembrane proton gradient. Quinol oxidase complexes such as the *Escherichia coli* cytochrome *bo* belong to this superfamily. To elucidate the similarities as well as differences between ubiquinol and cytochrome *c* oxidases, we have analysed two-dimensional crystals of cytochrome *bo* by cryo-electron microscopy. The crystals diffract beyond 5 Å. A projection map was calculated to a resolution of 6 Å. All four subunits can be identified and single α-helices are resolved within the density for the protein complex. The comparison with the three-dimensional structure of cytochrome *c* oxidase shows the clear structural similarity within the common functional core surrounding the metal-binding sites in subunit I. It also indicates subtle differences which are due to the distinct subunit composition. This study can be extended to a three-dimensional structure analysis of the quinol oxidase complex by electron image processing of tilted crystals.

Keywords: cytochrome *c* oxidase/electron microscopy/membrane protein structure/quinol oxidase/two-dimensional crystallization

Introduction

Haem–copper oxidases are terminal enzymes in the respiratory chain and catalyse the reduction of molecular oxygen to water by electrons originally deriving from the reduction of NADH or succinate by the electron transfer chain. During this reaction, protons are pumped across the membrane, leading to the generation of a chemiosmotic proton gradient which drives ATP synthesis (Trumpower and Gennis, 1994). The superfamily of haem–copper oxidases is divided into several branches (Castresana *et al.*, 1994; García-Horsman *et al.*, 1994; Castresana and Saraste, 1995). Mitochondrial cytochrome oxidases and most oxidases from aerobic bacteria use cytochrome *c* as a substrate, but many bacteria express homologous enzymes that use quinols as electron donor. The eukaryotic cytochrome *c* oxidase complex contains up to 13 different subunits, three of which are encoded by the mitochondrial DNA. The corresponding bacterial enzymes have a much simpler subunit composition, typically consisting of three or four subunits that always include one or more homologues of the mitochondrially coded eukaryotic proteins (Saraste, 1990).

The Gram-negative eubacterium *Escherichia coli* possesses a branched respiratory chain. Depending on the growth conditions, ubiquinol-8 is oxidized by molecular oxygen either by the cytochrome *bd* or the cytochrome *bo* complex. Only the cytochrome *bo* ubiquinol oxidase (hereafter referred to as Cyt *bo*) is a member of the haem–copper oxidase family. Neither cytochrome *c* reductase nor cytochrome *c* oxidase are present in *E.coli* (Anraku and Gennis, 1987). Similarly to the mitochondrial cytochrome *c* oxidase, Cyt *bo* generates a proton motive force (Kita *et al.*, 1982) by a combination of a scalar mechanism and a proton pump coupled to the redox chemistry (Puustinen *et al.*, 1989).

The genes for Cyt *bo* are organized in a single operon. Five open reading frames, *cyoABCDE*, encode the subunits II, I, III and IV of the complex and a protohaem IX farnesyltransferase, respectively (Chepuri *et al.*, 1990; Saiki *et al.*, 1992). Subunits I–III are homologous (10–40% identity) to the major subunits of the mitochondrial and bacterial cytochrome *c* oxidases (Chepuri *et al.*, 1990; Saraste, 1990), but subunit IV shows no homology to any component of the latter (Chepuri *et al.*, 1990; Haltia *et al.*, 1994).

Cyt *bo* can be purified as an intact protein complex, containing all four subunits (Matsushita *et al.*, 1984; Georgiou *et al.*, 1988). It contains two haem groups, which are haems B and O (Puustinen and Wikström, 1991). Additionally, about one copper atom is present per complex (Kita *et al.*, 1984). Haem B is in a low-spin configuration, and the high-spin haem O is antiferromagnetically coupled to the copper atom, called Cu_B (Salerno *et al.*, 1990). The iron of haem O and Cu_B form a binuclear centre in which oxygen is reduced. All metal centres reside in subunit I, CyoB (see Brown *et al.*, 1993; García-Horsman *et al.*, 1994). Using site-directed mutagenesis, the axial ligands to the metal centres have been identified as six invariant histidines in this subunit (Minagawa *et al.*, 1992; Lemieux *et al.*, 1992; Calhoun *et al.*, 1993; Uno *et al.*, 1994; Tsubaki *et al.*, 1994).

The three-dimensional structures are known for the cytochrome oxidases from *Paracoccus denitrificans* (Iwata *et al.*, 1995) and bovine heart mitochondria (Tsukihara *et al.*, 1995, 1996). The primary electron acceptor site Cu_A centre is present in the subunit II of cytochrome *c* oxidases but not in the corresponding subunit of quinol-oxidizing enzymes. However, it has been possible to engineer this metal centre into subunit II (CyoA) of Cyt *bo* (van der Oost *et al.*, 1992). The crystal structure of the periplasmic domain of CyoA, with and without the engineered copper site, has been determined at high resolution (Wilmanns *et al.*, 1995). Recent studies indicate

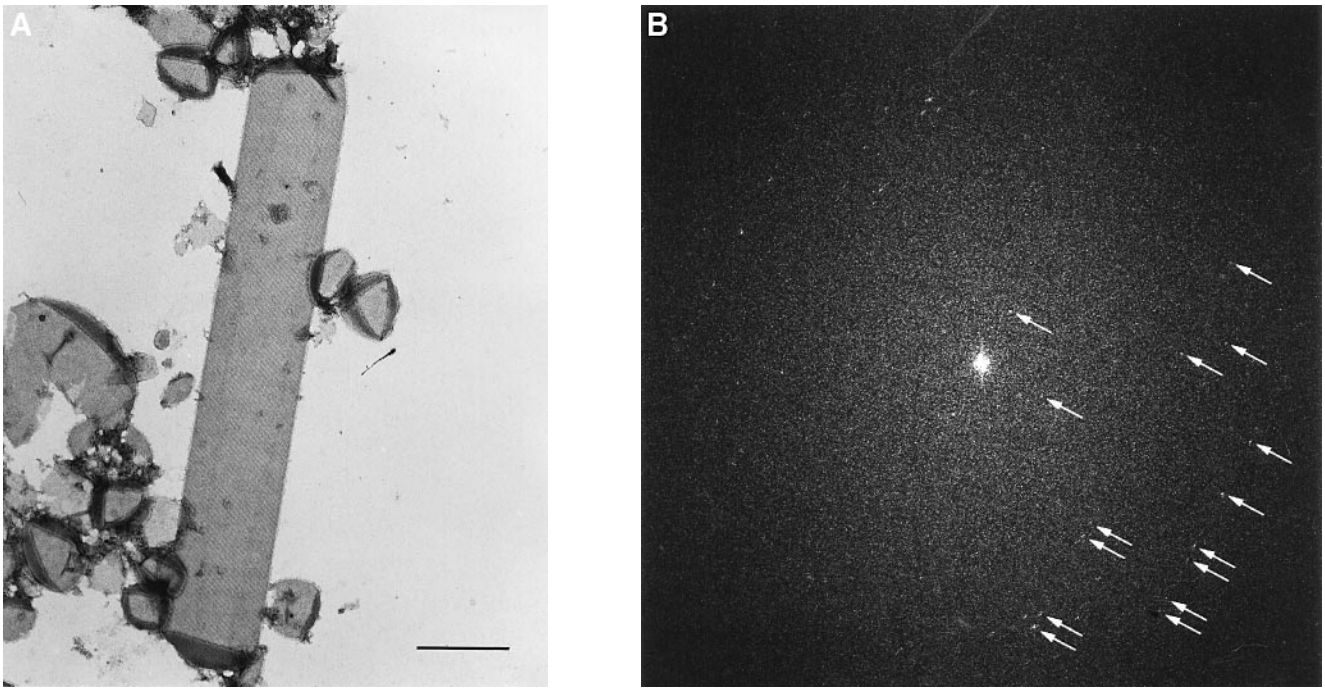

Fig. 1. (**A**) Tubular crystal of Cyt *bo* from *E.coli*. The crystal has been negatively stained with uranyl acetate. Scale bar represents 0.5 μm. (**B**) Computed diffraction pattern taken from a crystal embedded in amorphous ice (image No. 1415).

that electron transfer from quinol to the low-spin cytochrome *b* in subunit I follows a similar path as from Cu_A to cytochrome *a* in cytochrome *c* oxidases (Sato-Watanabe *et al.*, 1995; Puustinen *et al.*, 1996).

The function of subunit III is unspecified for all haem–copper oxidases. However, subunit III appears to be at least involved in the assembly of the complex (Haltia *et al.*, 1989). It has been suggested to play a role as an oxygen store (Tsukihara *et al.*, 1996), and to be part of the putative oxygen channel that leads to the binuclear centre (Riistama *et al.*, 1996). Likewise, the role of subunit IV is unknown. Preparations of bacterial cytochrome oxidase that consist of only subunits I and II are fully active (Hendler *et al.*, 1991). However, deletion of the gene encoding subunit IV impairs functional expression, probably due to defective assembly of the binuclear centre (Saiki *et al.*, 1996).

Structural studies on two-dimensional crystals of cytochrome *c* oxidases have been carried out for many years (see references in Frey, 1994). Three-dimensional models for the mitochondrial enzyme complex have been obtained at low resolution both in negative stain and amorphous ice (Deatherage *et al.*, 1982; Valpuesta *et al.*, 1990). Until now, structural details of a quinol oxidase complex have not been reported, apart from the three-dimensional structure of the periplasmic domain of CyoA (Wilmanns *et al.*, 1995). Here, we describe the projection structure of the entire Cyt *bo* complex determined by cryo-electron microscopy. The projected density in the membrane plane can be compared easily with the similarly oriented structure of the bacterial cytochrome *c* oxidase (Iwata *et al.*, 1995).

Results

Crystallization of Cyt bo and image processing

Two-dimensional crystallization studies on haem–copper oxidases have been carried out with cytochrome *c* oxidases purified from *P.denitrificans* and *Rhodobacter sphaeroides* and Cyt *bo* from *E.coli*. These enzymes form membraneous crystals which diffract to a resolution of ~25 Å in negative stain (Warne *et al.*, 1995). The best results in terms of crystal size and intrinsic order could be obtained with Cyt *bo* in which subunits II and I are genetically fused.

We have studied large flattened tubular crystals with dimensions of 0.5 μm in width and 2–8 μm in length by cryo-electron microscopy. Optical diffraction of the micrographs revealed reflections to a resolution of ~8 Å (Figure 1). After filtering and unbending of the crystal lattice (see Materials and methods), the Fourier transform of a single image could be obtained (Figure 2). Reflections from only one layer of the flattened tubular crystal can be observed from this image. The most likely reason for this on a holey carbon grid is that one of the two layers is disordered. In the air–ice interface this could be caused by a partial denaturation of the protein, while in the layer opposite to the air–water interface disorder could be caused by insufficient flattening of the lattice due to missing surface tension. In contrast, images taken from specimens in thinner ice on continuous carbon films show diffraction from both layers which can be processed separately (data not shown).

In Figure 2, reflections with an IQ value (see legend) of 3 or better are visible to a resolution of 5 Å. Comparison of the phases of all structure factors revealed the planar space group to be $p22_12_1$. The amplitudes and phases of the image were then averaged with symmetry applied, and amplitudes sharpened by a resolution-dependent scale factor (see Materials and methods). Table I shows the mean phase error of the averaged data in resolution ranges for 255 unique structure factors. The average error of the phases is less than random to a resolution of 6.0 Å.

Structure of the $p22_12_1$ crystal form

Figure 3 shows the projection map calculated using data obtained from a single two-dimensional crystal. Our inter-

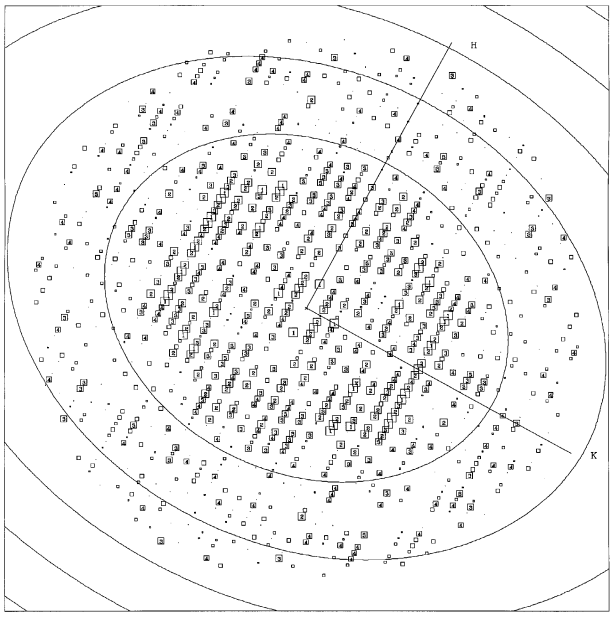

Fig. 2. Fourier transform of image No. 1415 after unbending of the crystal lattice. The squares indicate the positions of the reflections, and the size of the squares denotes the IQ value. The IQ is defined by 7/grade with grade being the signal-to-noise ratio of the reflection amplitude, i.e. grade = 1–7 (Henderson *et al.*, 1986). Spots of grade 8 are above background by an amount less than the background and are indicated by dots. The circles represent the zero values of the phase contrast transfer function. The resolution at the edge of the plot is 4.5 Å.

pretation is that, as the positive density represents protein mass, the asymmetric unit contains one Cyt *bo* complex (four asymmetric units per unit cell). The oxidase complexes seem to form dimers related by a crystallographic 2-fold axis perpendicular to the membrane plane. In the lattice, these dimers are oriented alternatively top-up and bottom-up, resulting in screw axes parallel to the membrane plane.

In Figure 4A, the projection map of the monomeric Cyt *bo* complex is shown. Although the identification and the assignment of secondary structure elements can be difficult in a projection map at medium resolution, the high quality of the data and the comparison with the X-ray structure of cytochrome *c* oxidase from *P.denitrificans* (Figure 4B; Iwata *et al.*, 1995) allows us to interpret the map as follows.

The complex consists of four subunits, namely the gene products of *cyoABCD*. The largest continuous density area in the map (Figure 4A) originates from subunits I and II (CyoB and CyoA). This density is recognizable by the pseudo 3-fold symmetry of subunit I (shaded yellow) that is known for cytochrome *c* oxidases (Iwata *et al.*, 1995; Tsukihara *et al.*, 1996). Within subunit I, several regions with negative density are found. They clearly correspond to the three pores found in cytochrome *c* oxidase (Iwata *et al.*, 1995). Pore A (bottom left) is blocked by mostly conserved aromatic residues, pore B (right) contains the binuclear centre and is covered by the periplasmic domain of subunit II, and pore C (top left and centre) ends at the cytochrome *b* centre (cytochrome *a* in cytochrome *c* oxidase). Positive density peaks typical for separate α-helices can hardly be resolved within subunit I, probably due to the fact that almost all α-helices in this subunit are tilted with respect to the membrane normal (cf. Iwata

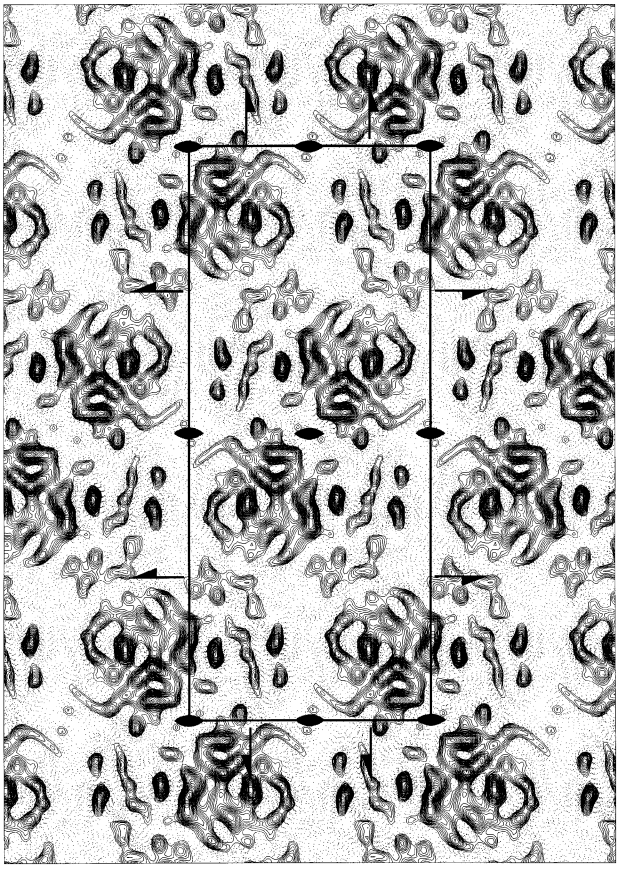

Fig. 3. Projection map with $p22_12_1$ symmetry calculated from amplitudes and phases of a single image (No. 1415) after processing. One unit cell (a = 200.65 Å, b = 85.92 Å) is outlined with the a-axis vertical and the b-axis horizontal. The map has been contoured in steps of 0.15× r.m.s. density. Negative density is indicated by dotted lines.

et al., 1995). The most prominent density that resembles an α-helix which is perpendicular to the membrane plane, divides pore C into two halves, and includes helix X and haem *b*. On the top-right of the molecule, two features are found that resemble a perpendicular and a largely tilted α-helix, respectively (shaded purple). Their arrangement matches almost exactly that of the two membrane-spanning helices of subunit II in cytochrome *c* oxidase (Figure 4B).

Assignment of the density found in the bottom part of the projection map (Figure 4A) is less straightforward. Analysis of the predicted sequences has shown that CyoB possesses one additional helix at the N-terminus (helix 0) and two additional helices in the C-terminus (helices XIII and XIV) in comparison with its homologue in cytochrome *c* oxidase (Chepuri and Gennis, 1990; Chepuri *et al.*, 1990). On the other hand, subunit III of Cyt *bo* (CyoC) consists of only five helices, whereas this subunit has seven helices in cytochrome *c* oxidase. Therefore, it is reasonable to assume that the arrangement of the last two C-terminal helices of subunit I in Cyt *bo* and the first two helices of subunit III in cytochrome *c* oxidase is similar. Hence, the density found in the bottom-left region of the map is assigned to helices XIII and XIV of CyoB (shaded yellow). Consequently, the right bottom part of the density probably corresponds to the five helices of CyoC (shaded blue).

Table I. Phase errors for image No. 1415 against 0 or 180° and figures of merit in resolution shells

Resolution range (Å)	No. of F_{Obs}	Mean value of $\Delta\alpha_C$ (°)	No. of standard deviations of mean below random (45°)	Mean figure of merit
200.0–22.5	20	22.3	4.5	0.86
22.5–16.0	22	23.6	4.3	0.85
16.0–13.5	17	19.0	6.1	0.90
13.5–11.5	23	19.7	6.0	0.89
11.5–10.0	31	10.4	17.0	0.97
10.0–8.0	47	32.3	3.1	0.75
8.0–7.0	40	39.6	1.4	0.70
7.0–6.0	55	43.4	0.5	0.67
Overall	255	29.6	9.7	0.79

All data with IQ values of 1–7 are included.
$\Delta\alpha_C$ is defined as the difference between the symmetry-imposed phase of 0 or 180° and the observed combined phase. Random phases would have a mean phase residual of 45° (Bullough and Tulloch, 1991). The figure of merit is defined as cos ($\Delta\alpha_C$).

The remaining density may be interpreted as subunit IV (CyoD, shaded green) which is predicted to have three membrane-spanning α-helices (Chepuri and Gennis, 1990). This is attached to subunits I and III in the region where the bacterial cytochrome *c* oxidase also contains an additional small subunit with a single transmembrane span (Iwata *et al.*, 1995; Figure 4C).

Discussion

The molecular anatomy of the complexes belonging to the two main branches of the haem–copper oxidase superfamily is very similar. In particular, the arrangement of metal centres and their surrounding transmembrane helices in subunit I and the folding of subunit II are well conserved. However, the fact that these two oxidase subgroups utilize completely different electron-donating substrates raises a question about structural differences between the quinol- and cytochrome *c*-oxidizing complexes. Cytochrome *c* is a soluble protein with a mol. wt of 12 000–14 000 Da. In contrast, the physiological electron donor for Cyo *bo*, ubiquinol, is a small, hydrophobic molecule with a mol. wt <1000 Da (727 Da for ubiquinol-8). Moreover, cytochrome *c* is an one-electron donor while ubiquinol is a two-electron donor.

The first proof for the high degree of similarity between cytochrome *c* and ubiquinol oxidases came from protein engineering studies on CyoA (van der Oost *et al.*, 1992). This was confirmed by the subsequent crystallographic studies (Iwata *et al.*, 1995; Tsukihara *et al.*, 1995, 1996; Wilmanns *et al.*, 1995). In relation to these studies, we have attempted to survey further structural similarities and possible differences by an electron crystallographic study on Cyt *bo*.

The projection structure of the entire Cyt *bo* at 6 Å resolution shows that the common subunit I–III segment has a similar fold to cytochrome *c* oxidase. The structure is very complex (25 predicted transmembrane helices; Chepuri and Gennis, 1990), and without additional information it would be extremely difficult to interpret. However, the known structure of cytochrome *c* oxidase from *P.denitrificans* (Iwata *et al.*, 1995) can be used as a template for analysis of the projection map. The comparison of both structures in projection (Figure 4) has made it possible to identify all four subunits of Cyt *bo* and, moreover, it allows the assignment of single α-helices. This is especially important in places where major differences occur between the primary structures. The first difference appears in subunit I (Figure 4A). This subunit in cytochrome *c* oxidase consists of 12 α-helices, whereas the corresponding CyoB subunit has been predicted to contain 15 transmembrane helices (Chepuri *et al.*, 1990; Ma *et al.*, 1993), which is supported by gene fusion experiments (Chepuri and Gennis, 1990). It is difficult to assign a particular density to the additional helix 0 at the N-terminus, although we assume that a weak peak of extra density on the left side of CyoB corresponds to this helix (Figure 4A, above left of pore A). It has been suggested that the two C-terminal helices of subunit I replace the first two helices of subunit III which are present in cytochrome *c* oxidase but missing in Cyt *bo* (Ma *et al.*, 1993). Although there is virtually no sequence homology between helices XIII and XIV of CyoB and helices I and II of subunit III in cytochrome *c* oxidase, the superposition of both projections (Figure 4C) indicates an almost identical arrangement of these helices in the membrane. This is supported by the fact that the Cyt *bo* complex, in which subunits I and III have been genetically fused, is fully active (Ma *et al.*, 1993). This swapping of a pair of transmembrane helices between subunits I and III is also known for the cytochrome *c* and quinol oxidases from *Bacillus* (Ishizuka *et al.*, 1990; Saraste *et al.*, 1991; Santana *et al.*, 1992). Finally, in the case of the cytochrome oxidases in *Thermus thermophilus* (Mather *et al.*, 1993) and *Sulfolobus acidocaldarius* (Lübben *et al.*, 1994), a natural genetic fusion between subunits I and III has occurred, possibly reflecting the high temperatures under which these thermophilic organisms live. The possibility of these fusions and swapping of terminal helices from subunit I to subunit III reflects the vicinity of the termini in the canonical 12-helix subunit I and the 7-helix subunit III.

The second difference between Cyt *bo* and bacterial cytochrome *c* oxidases is predicted to involve subunit IV (CyoD). Subunit IV of cytochrome *c* oxidase from *P.denitrificans* contains a single transmembrane helix (Iwata *et al.*, 1995), whereas hydropathy analysis and topological studies on CyoD have indicated three membrane-spanning helices (Chepuri and Gennis, 1990; Chepuri *et al.*, 1990). Cross-linking studies propose a close proximity of subunit IV to the subunits I and III (Saiki *et al.*, 1996).

Superposition of the lower regions of Cyt *bo* and

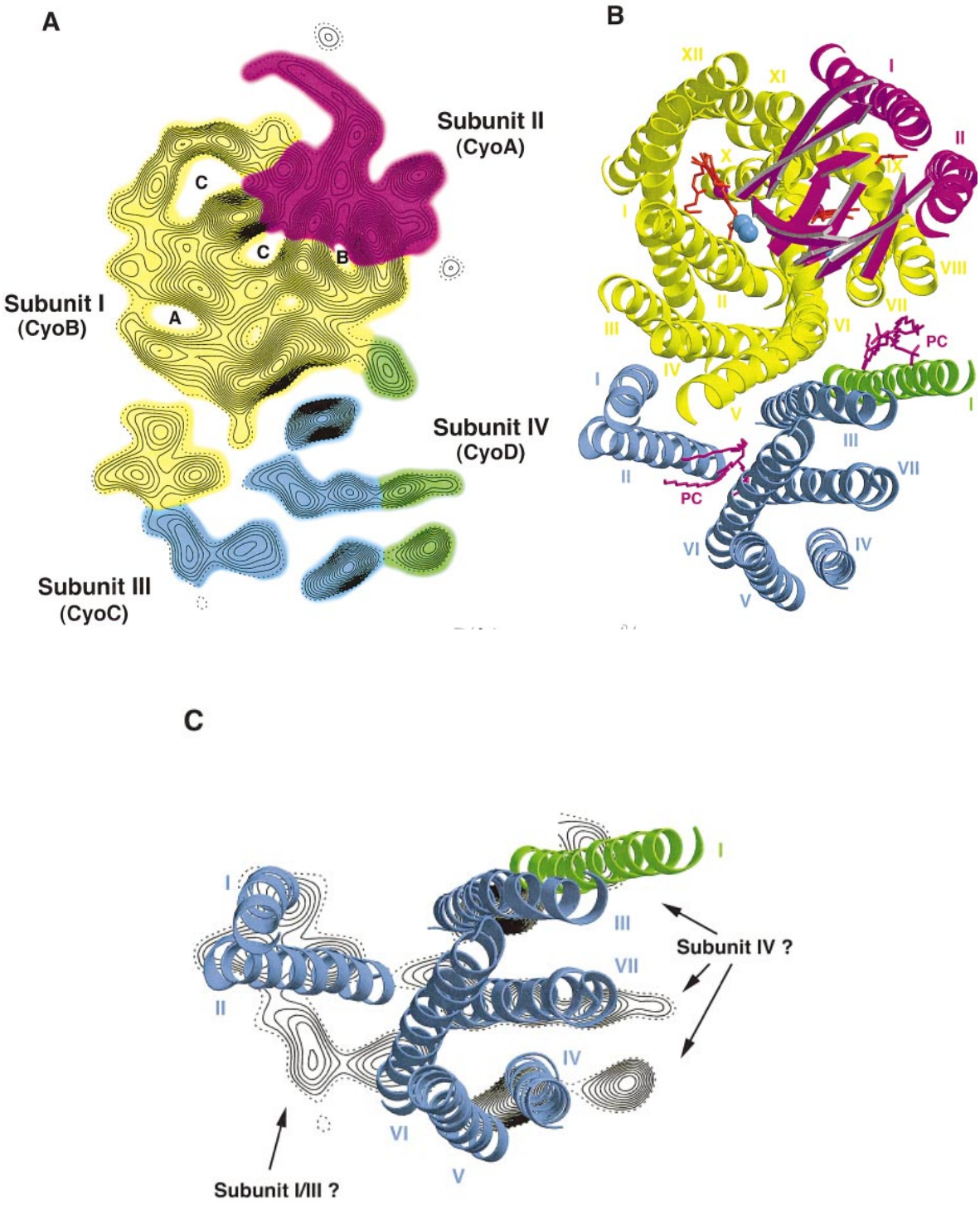

Fig. 4. (**A**) Projection map of a single Cyt *bo* complex at a resolution of 6 Å extracted from Figure 3. Contour levels are as in Figure 3 without negative density being shown. Dotted contours indicate the zero density level. The coloured shading represents the assignment of the four subunits of Cyt *bo* after comparison with the X-ray structure of cytochrome *c* oxidase (see B): subunit I, yellow; subunit II, purple; subunit III, blue and subunit IV, green. Three pores (see text) are labelled A, B and C. The figure was prepared with Adobe Photoshop. (**B**) Model of cytochrome *c* oxidase from *P.denitrificans*. The original structure was determined by the analysis of three-dimensional crystals at a resolution of 2.8 Å (Iwata *et al.*, 1995). Transmembrane helices (Roman numbering), as well as prosthetic groups and two firmly bound phospholipid molecules are shown. The view of the complex is along the membrane normal from the periplasmic side. The ribbon representation is coloured as in (A). The figure was generated with Molscript (Kraulis, 1991) and Raster3D (Bacon and Anderson, 1988; Merritt and Murphy, 1994). (**C**) Tentative assignment of subunit IV to the density of Cyt *bo* (see text). Colours are as in (B).

cytochrome *c* oxidase shows indeed that after the assignment of the C-terminal part of CyoB and five helices of CyoC, extra density remains which can account for the three α-helices of CyoD (Figure 4C). One of these density patches superimposes almost exactly with the position of the single transmembrane helix of subunit IV of cytochrome *c* oxidase. The remaining density appears to be closely attached to subunit III and is assigned to the

other transmembrane helices of CyoD. Between the C-terminus of subunit I and subunit III, a peak of density remains unassigned at the resolution of 6 Å (Figure 4C).

The detectable density for CyoA shows a striking similarity to the structure of the corresponding subunit II in cytochrome *c* oxidase. Subunit II consists of two membrane-spanning helices plus a large periplasmic domain (Iwata *et al.*, 1995). In both structures, the transmembrane helices appear to be oriented either tilted (helix I) or perpendicular (helix II) with respect to the membrane normal. There is no distinctive density for the cytoplasmic part of subunit II. This part of the polypeptide is folded as an 11-stranded β-sandwich followed by three short α-helices (Wilmanns *et al.*, 1995). While no distinct secondary structure can be expected for a β-sheet at 6 Å resolution, α-helices can already be resolved at medium resolution (Unwin and Henderson, 1975; Unwin, 1993). Extending the information obtained from the X-ray structures (Iwata *et al.*, 1995; Wilmanns *et al.*, 1995), our electron crystallographic data confirm that the transmembrane part of subunit II is also structurally conserved. Additionally, the mutual arrangement of subunits I and II is likely to be the same in both oxidase subfamilies.

Cytochrome *c* binds to the periplasmic surface of the cytochrome *c* oxidase. A part of its binding site is known to reside on the exposed region of subunit II (Taha and Ferguson-Miller, 1992; Lappalainen *et al.*, 1995). For ubiquinol oxidases the situation must be different. Accounting for the hydrophobic nature of the substrate, the binding site is thought to be located within the hydrophobic interior of the membrane bilayer. Studies with a photoreactive radiolabelled substrate analogue have indicated that subunit II is at least partially involved in ubiquinol binding (Welter *et al.*, 1994). Our future experiments will aim at the identification of this substrate-binding site by using gold-labelled ubiquinol derivatives. The combination of electron crystallography and gold-labelled substrates or polypeptides has been used already in studies on the localization of the cytochrome *c* binding site of mitochondrial oxidase (Frey and Murray, 1994) and the location of subunit III in the same complex (Crum *et al.*, 1994). Furthermore, our structural analysis will be extended to the recording of tilt series in order to obtain three-dimensional data of the Cyt *bo* complex. A three-dimensional model even at medium resolution will facilitate the interpretation of density maps and render a more accurate comparison possible with the available X-ray data of cytochrome *c* oxidases.

Phylogenetic analysis (Castresana *et al.*, 1994; van der Oost *et al.*, 1994; Castresana and Saraste, 1995) has led to the suggestion that the first cytochrome *c* oxidase containing B- and C-type haems evolved from a structurally similar nitric oxide reductase already under the primordial conditions when only a limited amount of free oxygen was present. This enzyme evolved to the mitochondrial-type cytochrome *c* oxidase by the incorporation of A-type haems and introduction of the Cu_A centre into subunit II. In a more recent step, the Cu_A centre was lost when the quinol oxidases developed in Eubacteria and Archaea. Our results show that both branches of the haem–copper oxidase family share the same fold, which confirms their common evolutionary history.

Materials and methods

Purification and crystallization

Purification and crystallization of Cyt *bo* from the *E.coli* strain RG129/pRCO1 was done as described (Warne *et al.*, 1995), with modifications. The strain overproduces an engineered Cyt *bo* with a genetic fusion between *cyo*A and *cyo*B encoding subunits II and I, respectively (Ma *et al.*, 1993). Two-dimensional crystallization was carried out by microdialysis (Warne *et al.*, 1995). Briefly, Cyt *bo* (1 mg/ml) was added to a 2.6:1 mixture of egg phosphatidylcholine and crude phosphatidylserine from bovine brain (Sigma, Germany) solubilized in Triton X-100 with a lipid to protein ratio of 0.29 by weight. Dialysis of 0.2% (w/v) detergent against 25 mM Tris, pH 9.0, containing 0.5 mM EDTA and 1 mM sodium azide at 37°C resulted in the formation of tubular crystals 2–8 μm in length. The use of pH 9.0–10.0 was essential for the formation of the tubes. The crystals were stable for at least 12 months at 4°C.

Cryo-electron microscopy

Aliquots (2.0 μl) of the crystal suspension were pipetted onto the grid side of copper grids covered with a holey carbon film. The excess liquid was then removed by blotting with filter paper from the carbon side, ensuring the trapping of the crystals across the holes (Toyoshima, 1989). Immediately, grids were plunged into a liquid ethane/liquid nitrogen slurry at a temperature of 93 K (Dubochet *et al.*, 1988). In the case of continuous carbon grids, 0.5 μl aliquots were applied to grids which had been glow-discharged in a pentylamine atmosphere. The specimens were then blotted and frozen as above. Finally, the grids were transferred under cryo conditions to either a Gatan- or an Oxford cold stage and examined on a JEOL 2000EX electron microscope operating at an accelerating voltage of 200 kV.

Images were selected by optical diffraction, based on a maximum resolution of 8–10 Å. Between 5% (holey carbon specimens) and 15% (continuous carbon grids) of ~200 recorded images were suitable for further processing. Areas showing good isotropic resolution were marked and digitized on a Perkin-Elmer 1010 M flat-bed microdensitometer. The size of the selected area was 3000×3000 pixels scanned with a circular aperture of 15 μm at a step size of 10 μm, corresponding to a pixel size of 2.5 Å (magnification 40 000×) at the specimen.

Image processing

The digitized images were processed using the MRC image processing programs (Crowther *et al.*, 1996). Briefly, the images were corrected for distortions of the crystal lattice, contrast transfer function (CTF), astigmatism and specimen drift (Henderson *et al.*, 1986). Manual indexing of the Fourier transform of the images revealed an orthorhombic planar space group with cell constants of $a = 200.65$ Å and $b = 85.92$ Å. This is in good agreement with the previous results with negatively stained crystals (space group $p22_12_1$, $a = 210$ Å, $b = 90$ Å, Warne *et al.*, 1995). The observed flattened tubes were not large enough for collecting electron diffraction data (width of the tubes ~0.5 μm). Therefore, the Fourier amplitudes were estimated from the image amplitudes. Comparison of the internal phase residual in all 17 space groups (Valpuesta *et al.*, 1994) revealed $p22_12_1$ symmetry for one image (No. 1415) and $p12_1$ symmetry for all other images examined so far (15 micrographs). The internal order of the lattice does not seem to be influenced by the space group since all processed images revealed structure factors to 6–8 Å. After refinement of the phase origin of image 1415 (using ORIGTILTD, Henderson *et al.*, 1986), the amplitudes and phases of symmetry-related reflections were averaged. The phases were rounded to either 0 or 180°, as the projection structure is centrosymmetric in this plane group. Finally, the image amplitudes were rescaled as a function of resolution to compensate for the loss of contrast caused by the limited intrinsic order of the crystals. The scale factors were derived from a comparison with the average amplitude of bacteriorhodopsin in projection at a given resolution (Havelka *et al.*, 1995).

Calculation of the projection map

With the amplitudes and phases obtained after the image processing, Fourier projection maps were calculated using the CCP4 program package (Collaborative Computational Project, No. 4, 1994). The structure factors were weighted by their figures of merit (Bullough and Tulloch, 1991).

Acknowledgements

We would like to thank M.Auer, M.Cyrklaff, B.Gowen, V.Guénebaut, W.Kühlbrandt, H.Savage and D.N.Wang at EMBL for their assistance

and advice with the early stages of electron microscopy and image processing. We are grateful to R.Henderson and N.Grigorieff at MRC-LMB, Cambridge, for discussion and invaluable comments, and to H.Michel, MPI für Biophysik, Frankfurt, for kindly making the co-ordinates of cytochrome *c* oxidase from *P.denitrificans* available to us. U.G. acknowledges financial support from EMBL.

References

Anraku,Y. and Gennis,R.B. (1987) The aerobic respiratory chain of *Escherichia coli*. *Trends Biochem. Sci*., **12**, 262–266.

Bacon,D.J. and Anderson,W.F. (1988) A fast algorithm for rendering space-filling molecule pictures. *J. Mol. Graphics*, **6**, 219–220.

Barton,G.J. (1993) ALSCRIPT: a tool to format multiple sequence alignments. *Protein Engng*, **6**, 37–40.

Brown,S., Moody,A.J., Mitchell,R. and Rich,P.R. (1993) Binuclear centre structure of terminal protonmotive oxidases. *FEBS Lett*., **316**, 216–223.

Bullough,P.A. and Tulloch,P.A. (1991) High resolution spot-scan electron microscopy of an α-helical coiled-coil protein. *J. Mol. Biol*., **215**, 161–173.

Calhoun,MW., Hill,J.J., Lemieux,L.J., Ingledew,W.J., Alben,J.O. and Gennis,R.B. (1993) Site-directed mutants of the cytochrome *bo* ubiquinol oxidase of *Escherichia coli*: amino acid substitutions for two histidines that are putative Cu_B ligands. *Biochemistry*, **32**, 11524–11529.

Castresana,J. and Saraste,M. (1995) Evolution of energetic metabolism: the respiration-early hypothesis. *Trends Biochem. Sci*., **20**, 443–448.

Castresana,J., Lübben,M., Saraste,M. and Higgins,D.G. (1994) Evolution of cytochrome oxidase, an enzyme older than atmospheric oxygen. *EMBO J*., **13**, 2516–2525.

Chepuri,V. and Gennis,R.B. (1990) The use of gene fusions to determine the topology of all of the subunits of the cytochrome *o* terminal oxidase complex of *Escherichia coli*. *J. Biol. Chem*., **265**, 12978–12986.

Chepuri,V., Lemieux,L., Au,D.C.-T. and Gennis,R.B. (1990) The sequence of the *cyo* operon indicates substantial structural similarities between the cytochrome *o* ubiquinol oxidase of *Escherichia coli* and the aa_3-type family of cytochrome *c* oxidases. *J. Biol. Chem*., **265**, 11185–11192.

Collaborative Computational Project, Number 4 (1991) The CCP4 suite: programs for protein crystallography. *Acta Crystallogr*., **D50**, 760–763.

Crowther,R.A., Henderson,R. and Smith,J.M. (1996) MRC image processing programs. *J. Struct. Biol*., **116**, 9–16.

Crum,J., Gruys,K.J. and Frey,T.G. (1994) Electron microscopy of cytochrome *c* oxidase crystals: labeling of subunit III with a monomaleimide undecagold cluster compound. *Biochemistry*, **33**, 13719–13726.

Deatherage,J.F., Henderson,R. and Capaldi,R.A. (1982) Three-dimensional structure of cytochrome *c* oxidase vesicle crystals in negative stain. *J. Mol. Biol*., **158**, 487–499.

Dubochet,J., Adrian,M., Chang,J.J., Homo.,J.C., Lepault,J., McDowell,A.W. and Schultz,P. (1988) Cryo-electron microscopy of vitrified specimens. *Q. Rev. Biochem*., **21**, 129–228.

Frey,T.G. (1994) Cytochrome *c* oxidase: structural studies by electron microscopy of two dimensional crystals. *Microsc. Res. Techn*., **27**, 319–332.

Frey,T.G. and Murray,J.M. (1994) Electron microscopy of cytochrome *c* oxidase crystals. *J. Mol. Biol*., **237**, 275–297.

García-Horsman,J.A., Barquera,B., Rumbley,J., Ma,J. and Gennis,R.B. (1994) The superfamily of haem–copper respiratory oxidases. *J. Bacteriol*., **176**, 5587–5600.

Georgiou,C.D., Cokic,P., Carter,K., Webster,D.A. and Gennis,R.B. (1988) Relationships between membrane-bound cytochrome *o* from *Vitreoscilla* and that of *Escherichia coli*. *Biochim. Biophys. Acta*, **933**, 179–183.

Haltia,T., Finel,M., Harms,N., Nakari,T., Raitio,M., Wikström,M. and Saraste,M. (1989) Deletion of the gene for subunit III leads to defective assembly of bacterial cytochrome oxidase. *EMBO J*., **8**, 3571–3579.

Haltia,T., Semo,N., Arrondo,J.L.R., Goñi,F.M. and Freire,E. (1994) Thermodynamic and structural stability of cytochrome *c* oxidase from *Paracoccus dentrificans*. *Biochemistry*, **33**, 9731–9740.

Havelka,W.A., Henderson,R. and Oesterhelt,D. (1995) Three-dimensional structure of halorhodopsin at 7 Å resolution. *J. Mol. Biol*., **247**, 726–738.

Henderson,R., Baldwin,J.M., Downing,K., Lepault,J. and Zemlin,F. (1986) Structure of purple membrane from *Halobacterium halobium*: recording, measurement, and evaluation of electron micrographs at 3.5 Å resolution. *Ultramicroscopy*, **19**, 147–178.

Hendler,R.W., Pardhasaradhi,K., Reynafarje,B. and Ludwig,B. (1991) Comparison of energy-transducing capabilities of the two- and three-subunit cytochromes aa_3 from *Paracoccus denitrificans* and the 13-subunit beef-heart enzyme. *Biophys. J*., **60**, 415–423.

Ishizuka,M., Machida,K., Shimada,S., Mogi,A., Tsuchiya,T., Ohmori,T., Souma,Y., Gonda,M. and Sone,N. (1990) Nucleotide sequence of the gene encoding for four subunits of cytochrome *c* oxidase from the thermophilic bacterium *PS3*. *J. Biochem*., **108**, 866–873.

Iwata,S., Ostermeier,C., Ludwig,B. and Michel,H. (1995) Structure at 2.8 Å resolution of cytochrome *c* oxidase from *Paracoccus denitrificans*. *Nature*, **376**, 660–669.

Kita,K., Kasahara,M. and Anraku,Y. (1982) Formation of a membrane potential by reconstituted liposomes made with cytochrome b_{562}–*o* complex, a terminal oxidase of *Escherichia coli* K12. *J. Biol. Chem*., **257**, 7933–7935.

Kita,K., Konishi,K. and Anraku,Y. (1984) Terminal oxidases of *Escherichia coli* aerobic respiratory chain. I. Purification and properties of cytochrome b_{562}–*o* complex from cells in the early exponential phase of aerobic growth. *J. Biol. Chem*., **259**, 3368–3374.

Kraulis,P. (1991) Molscript: a program to produce both detailed and schematic plots of proteins. *J. Appl. Crystallogr*., **24**, 946–950.

Lappalainen,P., Watmough,N.J., Greenwood,C. and Saraste,M. (1995) Electron transfer between cytochrome *c* and the isolated Cu_A domain: identification of substrate-binding residues in cytochrome *c* oxidase. *Biochemistry*, **34**, 5824–5830.

Lemieux,L.J., Calhoun,M.W., Thomas,J.W., Ingledew,W.J. and Gennis,R.B. (1992) Determination of the ligands of the low-spin haem of the cytochrome *o* ubiquinol oxidase complex using site-directed mutagenesis. *J. Biol. Chem*., **267**, 2105–2113.

Lübben,M., Arnaud,S., Castresana,J., Warne,A., Albracht,S.P.J. and Saraste,M. (1994) A second terminal oxidase in *Sulfolobus acidocaldarius*. *Eur. J. Biochem*., **224**, 151–159.

Ma,J., Lemieux,L. and Gennis,R.B. (1993) Genetic fusion of subunits I, II, and III of the cytochrome *bo* ubiquinol oxidase from *Escherichia coli* results in a fully assembled and active enzyme. *Biochemistry*, **32**, 7692–7697.

Mather,M.W., Springer,P., Hensel,S., Buse,G. and Fee,J.A. (1993) Cytochrome *c* oxidase from *Thermus thermophilus*. *J. Biol. Chem*., **268**, 5395–5408.

Matsushita,K., Patel,L. and Kaback,H.R. (1984) Cytochrome *o* type oxidase from *Escherichia coli*. Characterization of the enzyme and mechanism of electrochemical proton gradient generation. *Biochemistry*, **23**, 4703–4714.

Merritt,E.A. and Murphy,M.E.P. (1994) Raster3D version 2.0—a program for photorealistic molecular graphics. *Acta Crystallogr*., **D50**, 869–873.

Minagawa,J., Mogi,T., Gennis,R.B. and Anraku,Y. (1992) Identification of haem ligands in subunit I of the cytochrome *bo* complex in *Escherichia coli*. *J. Biol. Chem*., **267**, 2096–2104.

Puustinen,A. and Wikström,M. (1991) The haem groups of cytochrome *o* from *Escherichia coli*. *Proc. Natl Acad. Sci. USA*, **88**, 6122–6126.

Puustinen,A., Finel,M., Virrki,M. and Wikström,M. (1989) Cytochrome *o* (*bo*) is a proton pump in *Paracoccus denitrificans* and *Escherichia coli*. *FEBS Lett*., **249**, 163–167.

Puustinen,A., Verkhovsky,M.L., Morgan,J.E., Belevich,N.P. and Wikström,M. (1996) Reaction of the *Escherichia coli* quinol oxidase cytochrome bo_3 with dioxygen: the role of a bound ubiquinone molecule. *Proc. Natl Acad. Sci. USA*, **9**3, 1545–1548.

Riistama,S., Puustinen,A., García-Horsman,A., Iwata,S., Michel,H. and Wikström,M. (1996) Channelling of dioxygen into the respiratory enzyme. *Biochim. Biophys. Acta*, **1275**, 1–4.

Saiki,K., Mogi,T. and Anraku,Y. (1992) Haem *o* biosynthesis in *Escherichia coli*. The *cyoE* gene in the cytochrome *bo* operon encodes a protohaem IX farnesyltransferase. *Biochem. Biophys. Res. Commun*., **189**, 1491–1497.

Saiki,K., Nakamura,H., Mogi,T. and Anraku,Y. (1996) Probing a role of subunit IV of the *Escherichia coli bo*-type ubiquinol oxidase by deletion and cross-linking analyses. *J. Biol. Chem*., **271**, 15336–15340.

Salerno,J.C., Bolgiano,B., Poole,R.K., Gennis,R.B. and Ingledew,W.J. (1990) Haem–copper and haem–haem interactions in the cytochrome *bo*-containing quinol oxidase of *Escherichia coli*. *J. Biol. Chem*., **265**, 4364–4368.

Santana,M., Kunst,F., Hullo,M., Rapoport,G., Danchin,A. and Glaser,P. (1992) Molecular cloning, sequencing, and physiological characterization of the *qox* operon from *Bacillus subtilis* encoding the aa_3-600 quinol oxidase. *J. Biol. Chem*., **267**, 10225–10231.

Saraste,M. (1990) Structural features of cytochrome oxidase. *Q. Rev. Biophys*., **23**, 331–366.

Saraste,M., Metso,T., Nakari,T., Jalli,T., Laureus,M. and van der Oost,J. (1991) The *Bacillus subtilis* cytochrome-*c* oxidase. *Eur. J. Biochem*., **195**, 517–525.

Sato-Watanabe,M., Itoh,S., Mogi,T., Matsura,K., Miyoshi,H. and Anraku,Y. (1995) Stabilization of a semiquinone radical at the high affinity quinone-binding site (QH) of the *Escherichia coli bo*-type ubiquinol oxidase. *FEBS Lett*., **374**, 265–269.

Taha,T.S.M. and Ferguson-Miller,S. (1992) Interaction of cytochrome *c* with cytochrome *c* oxidase studied by monoclonal antibodies and protein modifiying agent. *Biochemistry*, **31**, 9090–9097.

Toyoshima,C. (1989) On the use of holey grids in electron crystallography. *Ultramicroscopy*, **30**, 439–444.

Trumpower,B.L. and Gennis,R.B. (1994) Energy transduction by cytochrome complexes in mitochondrial and bacterial respiration. *Annu. Rev. Biochem*., **63**, 675–716.

Tsubaki,M., Mogi,T., Hori,H., Hirota,S., Ogura,T., Kitagawa,T. and Anraku,Y. (1994) Molecular structure of redox metal centers of the cytochrome *bo* complex from *E.coli*. *J. Biol. Chem*., **269**, 30861–30868.

Tsukihara,T., Aoyama,H., Yamashita,E., Tomizaki,T., Yamaguchi,H., Shinzawa-Itoh,K., Nakashima,R., Yaono,R. and Yoshikawa,S. (1995) Structures of metal sites of bovine heart cytochrome *c* oxidase at 2.8 Å. *Science*, **269**, 1069–1074.

Tsukihara,T., Aoyama,H., Yamashita,E., Tomizaki,T., Yamaguchi,H., Shinzawa-Itoh,K., Nakashima,R., Yaono,R. and Yoshikawa,S. (1996) The whole structure of the 13 subunit oxidized cytochrome *c* oxidase at 2.8 Å. *Science*, **272**, 1136–1144.

Uno,T., Mogi,T., Tsubaki,M., Nishimura,Y. and Anraku,Y. (1994) Resonance Raman and Fourier transform infrared studies on the subunit I histidine mutants of the cytochrome *bo* complex in *Escherichia coli*. *J. Biol. Chem*., **269**, 11912–11920.

Unwin,N. (1993) Nicotinic acetylcholine receptor at 9 Å resolution. *J. Mol. Biol*., **229**, 1101–1124.

Unwin,N. and Henderson,R. (1975) Molecular structure determination by electron microscopy of unstained crystalline specimens. *J. Mol. Biol*., **94**, 425–440.

Valpuesta,J.M., Henderson,R. and Frey,T.G. (1990) Electron cryo-microscopic analysis of crystalline cytochrome oxidase. *J. Mol. Biol*., **214**, 237–251.

Valpuesta,J.M., Carrascosa,J.L. and Henderson,R. (1994) Analysis of electron microscope images and electron diffraction patterns of thin crystals of Ø29 connectors in ice. *J. Mol. Biol*., **240**, 281–287.

van der Oost,J. *et al*. (1992) Restoration of a lost metal-binding site: construction of two different copper sites into a subunit of the *E.coli* cytochrome *o* quinol oxidase complex. *EMBO J*., **11**, 3209–3217.

van der Oost,J., de Boer,A.P.N., de Gier,J.W.L., Zumft,W.G., Stouthamer,A.H. and van Spanning,R.J.M. (1994). The heme–copper oxidase family consists of three distinct types of terminal oxidases and is related to nitric oxide reductase. *FEMS Microbiol. Lett*., **121**, 1–10.

Warne,A., Wang,D.N. and Saraste,M. (1995) Purification and two-dimensional crystallization of bacterial cytochrome oxidases. *Eur. J. Biochem*., **234**, 443–451.

Welter,R., Gu,L.-Q., Yu,L., Yu,C.A, Rumbley,J. and Gennis,R.B. (1994) Identification of the ubiquinol-binding site in the cytochrome bo_3-ubiquinol oxidase of *Escherichia coli*. *J. Biol. Chem*., **269**, 28834–28838.

Wilmanns,M., Lappalainen,P., Kelly,M., Sauer-Eriksson,E. and Saraste,M. (1995) Crystal structure of the membrane-exposed domain from a respiratory quinol oxidase complex with an engineered dinuclear copper center. *Proc. Natl Acad. Sci. USA*, **92**, 11955–11959.

Received on October 2, 1996; revised on November 11, 1996